Bioconjugate Chemistry

Article

pubs.acs.org/bc

# Electroactive Organic Dye Incorporating Dipeptides in the Formation of Self-Assembled Nanofibrous Hydrogels

Yu-Hao Liu, Shu-Min Hsu, Fang-Yi Wu, Hsun Cheng, Mei-Yu Yeh, and Hsin-Chieh Lin*

Department of Materials Science and Engineering, National Chiao Tung University, Hsinchu, 300, Taiwan, Republic of China

Supporting Information

**ABSTRACT:** In this study, we examined the self-assembly of four dipeptides conjugated with the electroactive dye naphthalenediimide (NDI). The presence of the NDI group at the N-terminus of Phe-Phe and Phe-Gly promoted the formation of one-dimensional (1-D) nanostructures and three-dimensional (3-D) colored hydrogels under both acidic and physiological conditions. The 1-D nanostructures of these gels were stabilized through intermolecular $\pi-\pi$ interactions of the conjugated systems and extended hydrogen bonding of the dipeptide units.


## INTRODUCTION

Supramolecular hydrogels, which feature a solid-like gel state arising from the self-assembly of small molecules in water, are potentially useful candidate materials in the rapidly expanding field of soft biomaterials.[1] Because the morphology of a supramolecular hydrogel is similar to that of the extracellular matrix in a biological tissue, supramolecular hydrogels form a particularly interesting class of biomaterials. Three major building blocks of supramolecular peptide hydrogels have been established previously: ionic complementary peptides,[2,3] peptide amphiphiles,[4,5] and low-molecular-weight hydrogels.[6,7] The latter have been explored for a variety of applications, including scaffolds for tissue engineering,[8−13] carriers for drug delivery,[6,14−19] matrices for enzyme assays,[7,20,21] fluorophores for biosensing,[22−24] and as topical agents for wound healing.[25,26] Recently, functional naphthalenediimide (NDI) dyes have been studied as key components in several systems, including polymeric solar cells,[27,28] polymer light-emitting diodes,[29] organic field effect transistors,[30−37] and ion sensors,[38,39] as well as in photodynamic therapy[40] and cell imaging.[38,41,42] In addition, NDI motifs have been employed as components in various (supra)molecular nanostructures, including catenanes, rotaxanes, barrels, and vesicles,[43−45] as well as one-dimensional (1-D) nanostructures (e.g., nanoribbons, nanofibers),[46,47] which can be used to construct more complex three-dimensional (3-D) materials (e.g., organogels,[48] hydrogels[47,49−51]).

In a microscopic sense, a 3-D supramolecular hydrogel is constructed through physical cross-linking and entanglement of self-assembled nanofibers, which themselves comprise units of molecular hydrogelators. An efficient strategy toward realizing a low-molecular-weight hydrogelator is to covalently bind a $\pi$-conjugated hydrophobic group to a short peptide.[52,53] In contrast to the symmetric NDI-peptide hydrogelators that have been investigated previously,[49] in this paper we report asymmetric NDI-capped hydrogelators formed from a hydrophobic octyl-capped NDI dye linked to dipeptides at the N-terminus. With this design, we constructed hydrogelators that could gel water under physiological conditions; indeed, our peptide/dye conjugates featuring the peptide sequences Phe-Phe and Phe-Gly underwent efficient self-assembly to form nanofibers and hydrogels in aqueous media at pH 7.4. In addition, we could use these water-soluble molecules for cell imaging at concentrations below their minimum gel concentration (mgc).

## RESULTS AND DISCUSSION

**Synthesis and Optical Properties.** We prepared the peptide/dye conjugates NDI-Phe-Phe (**1**), NDI-Phe-Gly (**2**), NDI-Gly-Phe (**3**), and NDI-Gly-Gly (**4**) through solid-phase peptide synthesis (SPPS) using 2-chlorotrityl chloride resin (Figure 1). Figure 2 presents the UV−vis absorption and fluorescence emission spectra of **1**−**4** in water (pH 7.4). The UV−vis spectra of **1**−**4** feature two bands centered at 236 nm

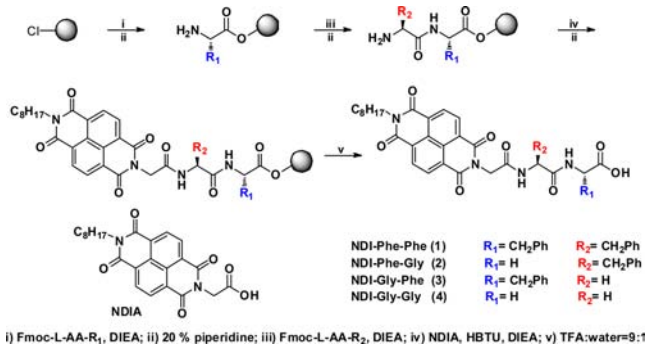


**Figure 1.** Synthesis of **1**−**4**.

**Received:** July 7, 2014
**Revised:** August 31, 2014
**Published:** September 17, 2014

  

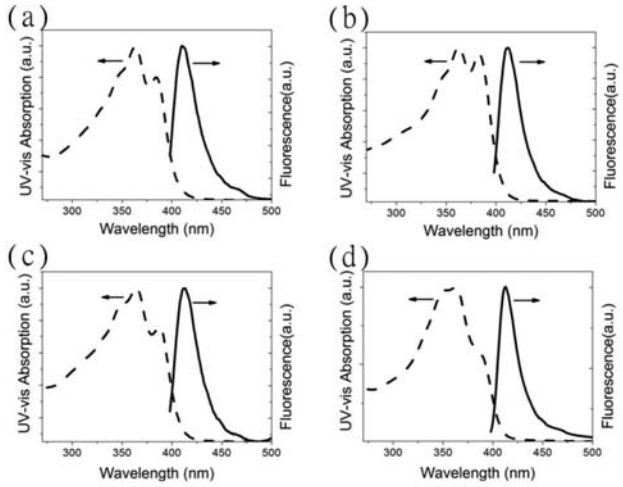


**Figure 2.** Normalized UV−vis absorption (dashed line) and fluorescence emission (solid line) spectra of (a) **1**, (b) **2**, (c) **3**, and (d) **4** (0.05 wt % in water).

(220−260 nm, band I) and 378 nm (320−410 nm, band II), consistent with $\pi-\pi^*$ transitions polarized along the short and long axes, respectively, of the NDI dye unit.[54] The emission spectra of aqueous solutions of **1**−**4**, recorded with excitation at a wavelength of 378 nm, each featured a clear emission band near 410 nm (i.e., in the visible region). Accordingly, we were interested in studying the cell imaging properties of **1**−**4**, using cultured MCF-7 cells as our test system.

After treating MCF-7 cells with the hydrogelators **1**−**4** (50 $\mu$M, 0.004 wt %) for 90 min, we observed blue-colored NDI fluorescence for the cells in the presence of **1** and **2**, but only weak fluorescence for those in the presence of **3** and **4** (Figure 3 and Supporting Information Figure S13). This result may be

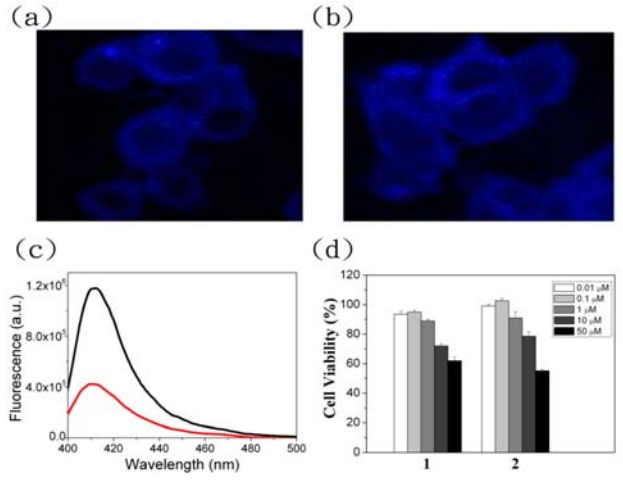


**Figure 3.** (a,b) Fluoresence images of MCF-7 cells incubated in the presence of (a) **1** and (b) **2** (50 $\mu$M) after 1.5 h. (c) Fluorescence emission spectra of **1** (red line) and **2** (black line) at 50 $\mu$M. (d) MCF-7 cell viability in the presence of **1** and **2** (0.1−50 $\mu$M).

attributed to the different hydrophobicity and amphiphilic properties of the hydrogelators.[55] These observations suggest that probes **1** and **2** were taken up by the MCF-7 cells, with **2** being a relatively better probe for cell imaging. This feature may be explained by the stronger fluorescent properties of **2** relative to that of **1** (Figure 3c). Furthermore, we tested **1** and **2** for their long-term biocompatibility with MCF-7 cells, using a colorimetric assay with 3-(4,5-dimethylthiazol-2-yl)-2,5-diphenyltetrazolium bromide (MTT). The concentrations of **1** and **2** required for 50% inhibition ($IC_{50}$) after 24 h were greater than 50 $\mu$M, suggesting acceptable biocompatibility for cell imaging. To study the cell uptake properties, we incubated MCF-7 cells with **1** and **2** at two concentrations (25 and 50 $\mu$M) and recorded fluorescence images over a period of 180 min (Supporting Information Figures S14−17). We observed that the fluorescent hydrogelators **1** and **2** entered the MCF-7 cells within 5 min, making them potentially efficient agents for cell imaging.

**Hydrogel Formation and Nanofiber Morphology.** We examined the self-assembly of the hydrogels through optical images recorded under acidic (insets to Figure 4) and

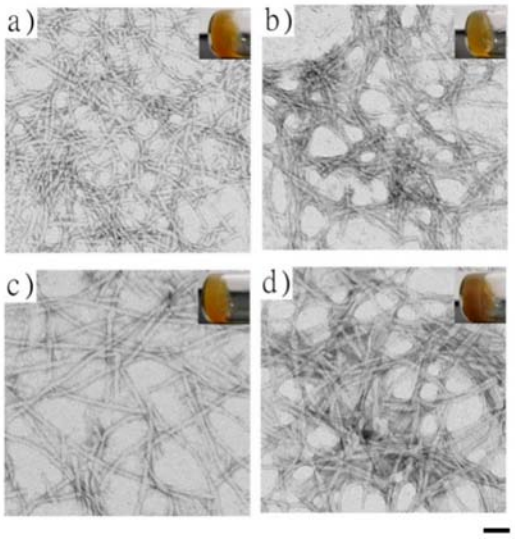


**Figure 4.** Optical microscopy and negatively stained TEM images of the hydrogels of (a) **1** (pH 4.8), (b) **2** (pH 4.7), (c) **3** (pH 4.3), and (d) **4** (pH 3.8), each at a concentration of 2 wt %. Scale bar: 50 nm.

physiological (insets to Figure 5) conditions. We used transmission electron microscopy (TEM) to observe the microscopic nanostructures of the peptide hydrogels (Figure 4). Under acidic conditions, **1**−**4** formed self-supporting hydrogels at a concentration of 2 wt % (Supporting Information Table S1). A decrease in the number of benzyl side chains in the dipeptide moiety resulted in hydrogelation at lower values of pH. TEM analysis revealed that the hydrogels of **1**−**4** featured uniform fibrous networks under acidic conditions, with these entangled nanofibers resulting in the trapping of water molecules.

Based on our success at forming NDI hydrogels under acidic conditions, we further examined the hydrogelation abilities of **1**−**4** under physiological conditions. We found that dissolving **1** or **2** at a concentration of 2 wt % in water at pH 7.4 led to the formation of a hydrogel (Figure 5, Table 1). The hydrogels of **1** and **2** appeared semitranslucent and transparent brownish, respectively, under physiological conditions. TEM images revealed that the hydrogels of **1** and **2** formed at pH 7.4 featured uniform fibrous networks. Thus, self-assembly and hydrogelation occurred for **1** and **2** under both acidic and physiological conditions. In contrast, **3** did not gel water at pH 7.4; the associated TEM image reveals the presence of bundle-like microscopic nanostructures (Figure 5c). Because **2** formed


dx.doi.org/10.1021/bc500299c | *Bioconjugate Chem.* 2014, 25, 1794−1800

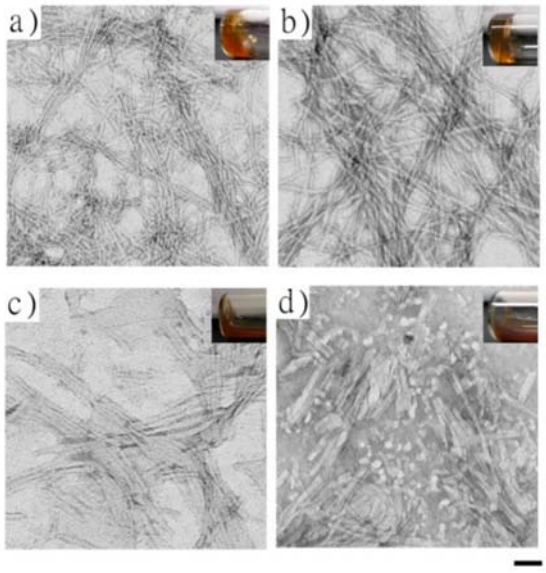


**Figure 5.** Optical microscopy and negatively stained TEM images of hydrogels of (a) **1**, (b) **2**, (c) **3**, and (d) **4** (concentration: 2 wt %; pH 7.4). Scale bar: 50 nm.

**Table 1. Physical Properties of NDI-Capped Dipeptides at 2 wt % and pH 7.4**

| entry | appr.[a] | $mgc$[b] (wt %) | $T_{gel-sol}$ (°C) | $G'$, $G''$ (Pa) | fiber diameter (nm) |
|---|---|---|---|---|---|
| **1** | SG | 0.47 | 60 | $1.6 \times 10^3$, $8.7 \times 10^1$ | 8 ± 1 |
| **2** | TG | 1.90 | >90[c] | $1.1 \times 10^3$, $2.4 \times 10^2$ | 8 ± 1 |
| **3** | TS | n.d. | n.d. | n.d. | 9 ± 2 |
| **4** | SS | n.d. | n.d. | n.d. | 10 ± 2 |

[a]appr.: appearance; SG: semitranslucent gel; TG: transparent gel; TS: transparent solution; SS: semitranslucent solution. [b]MGC: minimum gel concentration. [c]Gel was stable under this temperature.

a hydrogel, but **3** did not, even though they have the same molecular weight, we suspect that the presence of an NDI-Phe unit was necessary to trigger effective hydrogelation at physiological pH.[56] Similar to **3**, the dipeptide **4** did not form a supramolecular hydrogel at pH 7.4 (Figure 5d). The formation of hydrogels from **1** and **2** under physiological conditions suggests that the direct attachment of a unit of the dye NDI to the N-terminus of a Phe residue is a valid means of designing new supramolecular hydrogelators for application as nanostructured biomaterials. Under physiological conditions, the MGCs were lowest for **1** and **2** (ca. 0.47 and 1.9 wt %, respectively), implying that the presence of hydrophobic side chains on the amino acid residues resulted in lower values of MGC. In addition to undergoing hydrogelation under physiological conditions, the gel-to-sol transition temperatures ($T_{gel-sol}$) of **1** and **2** at 2 wt % were both above 37 °C (Table 1), suggesting potentially useful applications in tissue engineering.[8−13] Statistical analysis of the TEM images of the hydrogels of **1** and **2** revealed that their nanofibers had uniform diameters of 8 ± 1 nm; these self-assembled nanofibers functioned as matrices to sustain the hydrogels.

**Rheometry.** Dynamic oscillatory techniques can be used to assess the viscoelastic properties of hydrogels.[13] Accordingly, we determined the rheological properties of the hydrogels of **1**−**4** that formed at a concentration of 2 wt % under various acidic conditions (Figure 6a, Supporting Information Table S1). All of these hydrogelators exhibited viscoelastic properties,

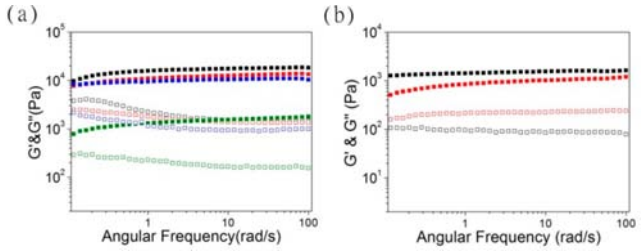


**Figure 6.** (a) Frequency sweeps of the hydrogels of **1** (pH 4.8), **2** (pH 4.7), **3** (pH 4.3), and **4** (pH 3.8). (b) Frequency sweeps of the hydrogels of **1** and **2** at pH 7.4. The hydrogels were prepared at 2 wt %; closed ($G'$) and open ($G''$) black squares for **1**, red squares for **2**, blue squares for **3**, and green squares for **4**.

as revealed by their storage moduli ($G'$) being higher than their loss moduli ($G''$). The storage moduli of **1**−**3** were all greater than 10 kPa, with that of the hydrogel of **1** being relatively higher than those of **2** and **3**. In comparison, the storage modulus of the hydrogel of **4** was significantly lower. These results suggest that the presence of a Phe residue imparted the fibrous networks of the hydrogels of **1**−**3** with resilience; in contrast, the lack of a benzyl side chain in **4** resulted in its hydrogel displaying relatively poor elastic properties. Thus, a correlation exists between the molecular structure and the viscoelasticity of these hydrogels.

Figure 6b and Table 1 present the viscoelastic properties of the hydrogels of **1** and **2** formed at pH 7.4. The storage moduli of the hydrogels of **1** and **2** were higher than their loss moduli, suggesting that these hydrogels were stable elastic materials. Comparing these two systems, we attribute the lower storage modulus for the hydrogel of **2** to its relative lack of aromatic moieties, thereby decreasing the number and strength of the noncovalent interactions required for stabilization of the self-assembled nanostructure and, thus, resulting in relatively weak viscoelastic properties for the hydrogel. Indeed, rheological tests suggested the importance of the aromatic moieties in the molecular aggregation and mechanical strength of the hydrogels under both acidic and physiological conditions. From our results, we suspect that the self-assembled nanostructures formed from NDI-capped dipeptides may function as 3-D scaffolds for cell growth. If a hydrogel is to provide a 3-D environment for cell growth, its mechanical properties should allow it to support the mass of a cell. Although the ideal storage modulus will vary depending on the type of cell, a storage modulus of approximately 100 Pa is the minimum required to support the mass of a cell.[35−37] The storage moduli of the hydrogels formed from **1** and **2** were greater than 1000 Pa; therefore, these materials can be viewed as potential 3-D materials for cell culturing. Modification of the peptide sequences will be required to ensure low cytotoxicity for such 3-D materials.

**Supramolecular Arrangement.** Spectroscopic characterization of hydrogelators in solution and in their gel states can provide valuable and relevant information regarding the intermolecular interactions present in their assemblies.[12,56] Figure 7 displays the spectroscopic features of **1** and **2** under physiological conditions. We recorded UV−vis absorption and circular dichroism (CD) spectra to study the intermolecular interactions and orientation of the $\pi$-conjugated chromophore

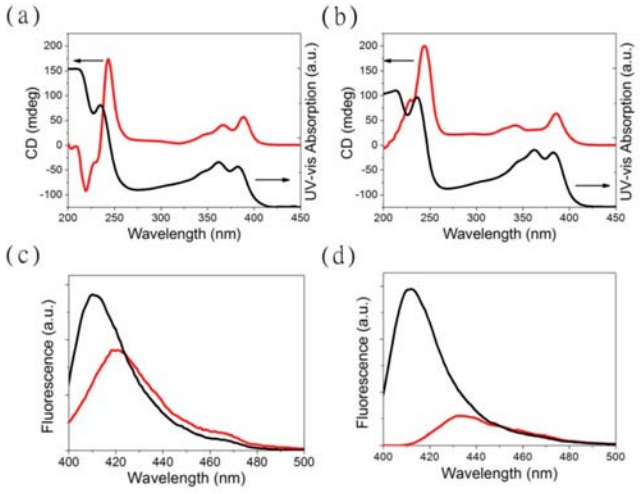


**Figure 7.** (a, b) CD (red line) and UV−vis absorption (black line) spectra of (a) **1** and (b) **2** (0.1 wt % in water). (c, d) Fluorescence emission spectra of (c) **1** and (d) **2** in the gel state (2 wt % in water, red line) and in solution (0.05 wt % in water, black line).

units in water. The CD spectrum of **1** reveals two excitonic Cotton effects for bands I and II. Interestingly, band I exhibited a bisignated Cotton effect centered at 238 nm, corresponding to a right-handed, P-type helical orientation in the assemblies. Notably, without changing the absolute configuration at the chiral centers, bands I and II in the CD spectrum of **1** are totally opposite sign to those for the M-type helical arrangement of NDI dyes in the system of Fmoc-KK(NDI).[47] Thus, the nanostructures formed by the NDI capping group at the N-terminus of the dipeptides had a P-type helical orientation; in contrast, the M-type helical structure was formed from Fmoc-KK(NDI), in which the NDI dye unit was capped in the side chain of the dipeptide.[47] In addition, the UV−vis and CD spectra of **2** revealed characteristics similar to those of **1**. In Figure 7c,d, we used the fluorescence emission to study the intermolecular $\pi-\pi$ interactions both in solution and in the gel state.[53] We recorded the emission spectra of **1** and **2** with excitation of the NDI chromophores at a wavelength 378 nm (determined from Figure 7a,b). Figure 7c reveals a clear emission band at 410 nm for **1** in solution; there appears to be a lower and red-shifted profile in the emission (ca. 421 nm) for the gel state of **1**, suggesting the occurrence of H-type aggregation. The hydrogel of **2** displayed (Figure 7d) more efficient emission quenching and a red-shifted peak (ca. 435 nm) relative to those of **1**, implying that the absence of the additional bulky benzyl side chain in **2** leads to compact packing of $\pi$-conjugated unit in the aggregates, which is consistent with the value of $T_{gel-sol}$ for the hydrogel of **2** being higher than that of **1** (Table 1).

The FTIR spectra of **1** and **2** reveal (Figure 8a) signals at 1630 and 1682 $cm^{-1}$, indicating the presence of $\beta$-sheet-like structures within their self-assembled nanofibers. In addition, two signals are present at 1667 and 1707 $cm^{-1}$, which we assign to symmetric and asymmetric stretching, respectively, of the imide C═O groups in the NDI moieties of **1** and **2**.[47] We employed wide-angle X-ray scattering (WAXS) to examine the structures of the hydrogels of **1** and **2** (Figure 8b). The scattering pattern of **1** (**2**) exhibited reflections near 3.54 (3.46) and 4.13 (4.33) Å, corresponding to the interplanar distance of stacked NDI chromophores and the interstrand distance between $\beta$-sheet superstructures, respectively. These spectroscopic features suggest the cooperative effect of $\pi-\pi$ interactions and hydrogen bonding as the major driving force behind the self-assembly of nanostructures from **1** and **2**. The spectroscopic data of **1**−**4** under acidic conditions (Supporting Information) were similar to those of **1** and **2** at pH 7.4.

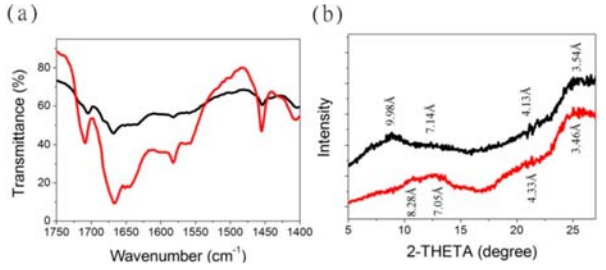


**Figure 8.** (a) FTIR spectra and (b) WAXS patterns of **1** (black) and **2** (red) in their gel states (2 wt %).

## CONCLUSION

We have developed a new system of low-molecular-weight hydrogelators prepared through the covalent linkage of the electroactive dye NDI to dipeptides. The appending of an NDI group at the N-terminus of Phe-Phe and Phe-Gly enhanced the formation of 1-D nanostructures and 3-D colored hydrogels under both acidic and physiological conditions. The 1-D nanostructures in the gels were stabilized through intermolecular $\pi-\pi$ interactions of the conjugated systems as well as extended hydrogen bonding of the dipeptide units. The storage moduli of the hydrogels formed from **1** and **2** were greater than 1000 Pa, suggesting that these materials can be viewed as potential 3-D materials for cell culturing. Alternatively, the electroactivity of the NDI component should be useful for investigations of conducting nanomaterials. In addition, the water-soluble compounds NDI-Phe-Phe and NDI-Phe-Gly functioned as contrast agents for cell imaging.

## EXPERIMENTAL PROCEDURES

**Synthesis of NDI-Phe-Phe (1).** The peptide/dye conjugate derivative of **1** was prepared through SPPS using 2-chlorotrityl chloride resin, Fmoc-L-phenylalanine, and NDIA (Figure 1).[57] The resin (0.6 g) was swelled in anhydrous $CH_2Cl_2$ for 30 min and then Fmoc-L-phenylalanine (0.3875 g, 1.000 mmol) was loaded onto the resin in anhydrous *N*,*N*-dimethylformamide and *N*,*N*-diisopropylethylamine (DIEA; 0.4150 mL, 2.500 mmol) for 1 h. For deprotection of the Fmoc group, piperidine (20% in DMF) was added and the sample left for 20 min; this procedure was repeated twice (each time for 2 min). Fmoc-L-phenylalanine (0.3875 g, 1.000 mmol) was coupled to the free amino group using *O*-(benzotriazol-1-yl)-*N*,*N*,*N*′,*N*′-tetramethyluraniumhexafluorophosphate (HBTU) (0.3793 g, 1.000 mmol) and *N*,*N*-diisopropylethylamine (DIEA) (0.4150 mL, 2.500 mmol) as coupling agents for 30 min. Again, the sample was treated with piperidine (20% in DMF) for 20 min; this procedure was repeated twice (each time for 2 min). Finally, NDIA (0.4365 g, 1.000 mmol) was coupled to the free amino group using HBTU (0.3793 g, 1.000 mmol) and DIEA (0.4150 mL, 2.500 mmol) as coupling agents. After the reaction mixture had been stirred overnight, the peptide derivative was cleaved through treatment with $CF_3CO_2H$ (90% in DI water) for 3 h. The resulting solution was dried by air and then $Et_2O$ was added to precipitate the target product. The solid was dried under vacuum to remove residual solvent (light-brown solid:


dx.doi.org/10.1021/bc500299c | *Bioconjugate Chem.* 2014, 25, 1794−1800

0.244 g). $^1$H NMR (300 MHz, [$D_6$]DMSO, 25 °C): $\delta$ 0.85−0.95 (m, 3H; $CH_3$), 1.20−1.45 (m, 10H; $CH_2$), 1.60−1.80 (m, 2H; $CH_2$), 2.70−3.15 (m, 4H; $CH_2$), 4.05−4.15 (m, 2H; $CH_2$), 4.40−4.55 (m, 1H; CH), 4.55−4.65 (m, 1H; CH), 4.70 (s, 2H; $CH_2$), 7.20−7.35 (m, 10H; CH), 8.40 (d, $J$ = 8.4 Hz, 1H; NH), 8.54 (d, $J$ = 7.5 Hz, 1H; NH), 8.65−8.80 (m, 4H; CH); $^{13}$C NMR (75 MHz, [$D_6$]DMSO, 25 °C): $\delta$ 14.0, 22.1, 26.5, 27.4, 28.6, 28.7, 31.3, 36.7, 37.6, 42.5, 53.6, 53.7, 125.9, 126.1, 126.3, 126.5, 126.6, 128.0, 128.2, 129.1, 129.3, 130.4, 130.7, 137.4, 137.6, 162.3, 162.6, 166.0, 170.9, 172.7; MS [FAB$^-$]: calcd. $m/z$ 730.30, obsvd. 729.8 $[M - H]^-$.

**Inverted Tube Method.** Gelation tests were performed by weighing a compound (2.0 mg) in a screw-capped 2 mL vial (diameter: 10 mm), adding a solvent (0.20 mL), sealing the vial tightly, heating it until the compound had dissolved, and then cooling the vial to room temperature. Gelation was considered to have occurred when a solid-like material was obtained that did not exhibit gravitational flow (inverted test tube method) during a period of 5 min. The MGC was determined after dilution of the sample with subsequent volumes of solvent (0.20 mL) until the gel material remained dissolved after heating.[58]

**Rheological Tests.** Rheological tests were conducted using an Anton Paar rheometer and a 25 mm parallel plate. The hydrogel sample (200 $\mu$L, 1 wt %) was placed on the parallel plate for the angular frequency sweep test (test range: 0.1 to 100 rad s$^{-1}$; strain, 0.8%; 13 points per decade; sweep mode, "log"; temperature, 25 °C).

**Cell Imaging.** MCF-7 cells were seeded in a 35 mm Petri dish equipped with a glass cover slide. After 12 h, the cells were stained with the peptides (50 $\mu$M) for 1.5 h. Prior to collecting imaging data, the cells were washed three times with phosphate-buffered saline (PBS, pH 7.4). Images were acquired using inverted fluorescence microscopy (Zeiss laser scanning microscope; DAPI filter; excitation: 350 nm; emission collected: 410−510 nm).

**MTT Assay.** The biocompatibilities of the peptides were measured by the MTT cell proliferation assay. MCF-7 cells were seeded in 24-well plates at a density of 50 000 cells per well with 0.5 mL DMEM contained 10% FBS and 1% penicillin and incubated for overnight. Compounds at different concentrations (0.01, 0.1, 1, 10, 50 $\mu$M) were added when cells were plated. Twenty-four hours later, the medium was replaced with 0.5 mL per well of fresh medium contained 10% MTT reagent (5 mg mL$^{-1}$). After 4 h of incubation at 37 °C in a 5% $CO_2$ incubator, the medium containing MTT was removed and DMSO was added to dissolve the formazan crystals and aliquots were pipetted into a 96-well plate. The optical density of the resulting solution was measured at 595 nm, using an absorbance microplate reader (Infinite F50, TECAN). Cells without the treatment of the compounds were used as the control. The cell viability percentage was calculated by the following formula:

$$\text{Cell viability percentage (\%)} = \text{OD}_{\text{sample}}/\text{OD}_{\text{control}} \times 100\%$$

## ■ ASSOCIATED CONTENT

### Supporting Information

Synthetic details and characterization data for **2**−**4**; NMR spectra of the hydrogelators **1**−**4**; spectroscopic characterization data recorded under acidic conditions; fluorescence images of MCF-7 cells in the presence of **3** and **4**. This material is available free of charge via the Internet at http://pubs.acs.org.

## ■ AUTHOR INFORMATION

### Corresponding Author

*Phone. +886-3-573-1949. E-mail: hclin45@nctu.edu.tw.

### Notes

The authors declare no competing financial interest.

## ■ ACKNOWLEDGMENTS

This study was supported financially by the National Science Council of the Republic of China, Taiwan (grant NSC 102-2113-M-009-006-MY2); the "Aim for the Top University" program of National Chiao Tung University; and the Ministry of Education, Taiwan, R.O.C. We thank the National Center for High-Performance Computing of Taiwan for computer time and facilities, and Professor Shiaw-Guang Hu for technical support.

## ■ REFERENCES

(1) Lin, H.-C., and Xu, B. (2012) *Applications of Supramolecular Chemistry* (Schneider, H.-J., Eds.) Chapter 13, CRC Press, Boca Raton.
(2) Zhang, S. (2012) Lipid-like self-assembling peptides. *Acc. Chem. Res. 45*, 2142−2150.
(3) Luo, Z., and Zhang, S. (2012) Designer nanomaterials using chiral self-assembling peptide systems and their emerging benefit for society. *Chem. Soc. Rev. 41*, 4736−4754.
(4) Hartgerink, J. D., Beniash, E., and Stupp, S. I. (2001) Self-assembly and mineralization of peptide-amphiphile nanofibers. *Science 294*, 1684−1688.
(5) Silva, G. A., Czeisler, C., Niece, C. K. L., Beniash, E., Harrington, D. A., Kessler, J. A., and Stupp, S. I. (2004) Selective differentiation of neural progenitor cells by high-epitope density nanofibers. *Science 303*, 1352−1355.
(6) Zhao, F., Ma, M. L., and Xu, B. (2009) Molecular hydrogels of therapeutic agents. *Chem. Soc. Rev. 38*, 883−891.
(7) Yang, Z., Liang, G., and Xu, B. (2008) Enzymatic hydrogelation of small molecules. *Acc. Chem. .Res. 41*, 315−326.
(8) Mahler, A., Reches, M., Rechter, M., Cohen, S., and Gazit, E. (2006) Rigid, self-assembled hydrogel composed of a modified aromatic dipeptide. *Adv. Mater. . 18*, 1365−1370.
(9) Holmes, T. C., de Lacalle, S., Su, X., Liu, G. S., Rich, A., and Zhang, S. G. (2000) Extensive neurite outgrowth and active synapse formation on self-assembling peptide scaffolds. *Proc. Natl. Acad. Sci. U.S.A. 97*, 6728−6733.
(10) Haines, L. A., Rajagopal, K., Ozbas, B., Salick, D. A., Pochan, D. J., and Schneider, J. P. (2005) Light-activated hydrogel formation via the triggered folding and self-assembly of a designed peptide. *J. Am. Chem. Soc. 127*, 17025−17029.
(11) Galler, K. M., Aulisa, L., Regan, K. R., D'Souza, R. N., and Hartgerink, J. D. (2010) Self-assembling multidomain peptide hydrogels: designed susceptibility to enzymatic cleavage allows enhanced cell migration and spreading. *J. Am. Chem. Soc. 132*, 3217−3223.
(12) Smith, A. M., Williams, R. J., Tang, C., Coppo, P., Collins, R. F., Turner, M. L., Saiani, A., and Ulijn, R. V. (2008) Fmoc-diphenylalanine self assembles to a hydrogel via a novel architecture based on $\pi$−$\pi$ interlocked $\beta$-sheets. *Adv. Mater. 20*, 37−41.
(13) Hsu, S.-M., Lin, Y.-C., Chang, J.-W., Liu, Y.-H., and Lin, H.-C. (2014) Intramolecular interactions of a phenyl/perfluorophenyl pair in the formation of supramolecular nanofibers and hydrogels. *Angew. Chem., Int. Ed. 53*, 1921−1927.
(14) Li, J., Kuang, Y., Gao, Y., Du, X., Shi, J., and Xu, B. (2013) D-Amino acids boost the selectivity and confer supramolecular hydrogels of a non-steroidal anti-inflammatory drug (NSAID). *J. Am. Chem. Soc. 135*, 542−545.

(15) Wang, H., Wei, J., Yang, C., Zhao, H., Li, D., Yin, Z., and Yang, Z. (2012) The inhibition of tumor growth and metastasis by self-assembled nanofibers of taxol. *Biomaterials 33*, 5848−5853.
(16) Li, X., Kuang, Y., Shi, J., Gao, Y., Lin, H.-C., and Xu, B. (2011) Multifunctional, biocompatible supramolecular hydrogelators consist only of nucleobase, amino acid, and glycoside. *J. Am. Chem. Soc. 133*, 17513−17518.
(17) Komatsu, H., Matsumoto, S., Tamaru, S., Kaneko, K., Ikeda, M., and Hamachi, I. (2009) Supramolecular hydrogel exhibiting four basic logic gate functions to fine-tune substance release. *J. Am. Chem. Soc. 131*, 5580−5585.
(18) Boekhoven, J., Koot, M., Wezendonk, T. A., Eelkema, R., and van Esch, J. H. (2012) A self-assembled delivery platform with post-production tunable release rate. *J. Am. Chem. Soc. 134*, 12908−12911.
(19) Kleinsmann, A. J., and Nachtsheim, B. J. (2013) Phenylalanine-containing cyclic dipeptides − the lowest molecular weight hydrogelators based on unmodified proteinogenic amino acids. *Chem. Commun. 49*, 7818−7820.
(20) Kiyonaka, S., Sada, K., Yoshimura, I., Shinkai, S., Kato, N., and Hamachi, I. (2004) Semi-wet peptide/protein array using supramolecular hydrogel. *Nat. Mater. 3*, 58−64.
(21) Yang, Z., Xu, K., Guo, Z., and Xu, B. (2007) Intracellular enzymatic formation of nanofibers results in hydrogelation and regulated cell death. *Adv. Mater. 19*, 3152−3156.
(22) Wada, A., Tamaru, S., Ikeda, M., and Hamachi, I. (2009) MCM−enzyme−supramolecular hydrogel hybrid as a fluorescence sensing material for polyanions of biological significance. *J. Am. Chem. Soc. 131*, 5321−5330.
(23) Rajagopalan, A., and Kroutil, W. (2011) Biocatalytic reactions: selected highlights. *Mater. Today 14*, 144−152.
(24) Bremmer, S. C., Chen, J., McNeil, A. J., and Soellner, M. B. (2012) A general method for detecting protease activity via gelation and its application to artificial clotting. *Chem. Commun. 48*, 5482−5484.
(25) Yang, Z., Liang, G., Ma, M., Abbah, A. S., Lu, W. W., and Xu, B. (2007) D-Glucosamine-based supramolecular hydrogels to improve wound healing. *Chem. .Commun.*, 843−845.
(26) Li, X., Kuang, Y., Lin, H.-C., Gao, Y., Shi, J., and Xu, B. (2011) Supramolecular nanofibers and hydrogels of nucleopeptides. *Angew. Chem., Int. Ed. 50*, 9365−9369.
(27) Earmme, T., Hwang, Y.-J., Murari, N. M., Subramaniyan, S., and Jenekhe, S. A. (2013) All-polymer solar cells with 3.3% efficiency based on naphthalene diimide-selenophene copolymer acceptor. *J. Am. Chem. Soc. 135*, 14960−14963.
(28) Schubert, M., Dolfen, D., Frisch, J., Roland, S., Steyrleuthner, R., Stiller, B., Chen, Z., Scherf, U., Koch, N., Facchetti, A., and Neher, D. (2012) Influence of aggregation on the performance of all-polymer solar cells containing low-bandgap naphthalenediimide copolymers. *Adv. Energy Mater. 2*, 369−380.
(29) Rozanski, L. J., Castaldelli, E., Sam, F. L. M., Mills, C. A., Demets, G. J.-F., and Silva, S. R. P. (2013) Solution processed naphthalene diimide derivative as electron transport layers for enhanced brightness and efficient polymer light emitting diodes. *J. Mater. Chem. C 1*, 3347−3352.
(30) Yan, H., Chen, Z., Zheng, Y., Newman, C., Quinn, J. R., Dotz, F., Kastler, M., and Facchetti, A. (2009) A high-mobility electron-transporting polymer for printed transistors. *Nature 457*, 679−686.
(31) Chang, J., Ye, Q., Huang, K.-W., Zhang, J., Chen, Z.-K., Wu, J., and Chi, C. (2012) Stepwise cyanation of naphthalene diimide for n-channel field-effect transistors. *Org. Lett. 14*, 2964−2967.
(32) Lee, W.-Y., Oh, J. H., Suraru, S.-L., Chen, W.-C., Würthner, F., and Bao, Z. (2011) High-mobility air-stable solution-shear-processed n-channel organic transistors based on core-chlorinated naphthalene diimides. *Adv. Funct. Mater. 21*, 4173−4181.
(33) Wurthner, F., and Stolte, M. (2011) Naphthalene and perylene diimides for organic transistors. *Chem. Commun. 47*, 5109−5115.
(34) Ortiz, R. P., Herrera, H., Blanco, R., Huang, H., Facchetti, A., Marks, T. J., Zheng, Y., and Segura, J. L. (2010) Organic n-channel field-effect transistors based on arylenediimide-thiophene derivatives. *J. Am. Chem. Soc. 132*, 8440−8452.
(35) Chen, Z., Zheng, Y., Yan, H., and Facchetti, A. (2009) Naphthalenedicarboximide- vs perylenedicarboximide-based copolymers. synthesis and semiconducting properties in bottom-gate n-channel organic transistors. *J. Am. Chem. Soc. 131*, 8−9.
(36) Katz, H. E., Lovinger, A. J., Kloc, C., Siegrist, T., Li, W., Lin, Y.-Y., and Dodabalapur, A. (2000) A soluble and air-stable organic semiconductor with high electron mobility. *Nature 404*, 478−481.
(37) Guo, X., Kim, F. S., Seger, M. J., Jenekhe, S. A., and Watson, M. D. (2012) Naphthalene diimide-based polymer semiconductors: synthesis, structure−property correlations, and n-channel and ambipolar field-effect transistors. *Chem. Mater. 24*, 1434−1442.
(38) Li, Q., Peng, M., Li, H., Zhong, C., Zhang, L., Cheng, X., Peng, X., Wang, Q., Qin, J., and Li, Z. (2012) Activation of the Si−B linkage: copper-catalyzed addition of nucleophilic silicon to imines. *Org. Lett. 14*, 2094−2097.
(39) Guha, S., and Saha, S. (2010) Fluoride ion sensing by an anion−$\pi$ interaction. *J. Am. Chem. Soc. 132*, 17674−17677.
(40) Doria, F., Manet, I., Grande, V., Monti, S., and Freccero, M. (2013) Water-soluble naphthalene diimides as singlet oxygen sensitizers. *J. Org. Chem. 78*, 8065−8073.
(41) Chang, S., Wu, X., Li, Y., Niu, D., Gao, Y., Ma, Z., Gu, J., Zhao, W., Zhu, W., Tian, H., and Shi, J. (2013) A pH-responsive hybrid fluorescent nanoprober for real time cell labeling and endocytosis tracking. *Biomaterials 34*, 10182−10190.
(42) Hu, Z., Pantoş, G. D., Kuganathan, N., Arrowsmith, R. L., Jacobs, R. M. J., Kociok-Köhn, G., O'Byrne, J., Jurkschat, K., Burgos, P., Tyrrell, R. M., Botchway, S. W., Sanders, J. K. M., and Pascu, S. I. (2012) Interactions between amino acid-tagged naphthalenediimide and single walled carbon nanotubes for the design and construction of new bioimaging probes. *Adv. Funct. Mater. 22*, 503−518.
(43) Fallon, G. D., Lee, M. A.-P., Langford, S. J., and Nichols, P. J. (2004) Unusual solid-state behavior in a neutral [2] catenane bearing a hydrolyzable component. *Org. Lett. 6*, 655−658.
(44) Hansen, J. G., Feeder, N., Hailton, D. G., Gunter, M. J., Becher, J., and Sanders, K. M. (2000) Macrocyclization and molecular interlocking via mitsunobu alkylation: highlighting the role of C−H···O interactions in templating. *Org. Lett. 2*, 449−452.
(45) Das, A., and Ghosh, S. (2013) Luminescent invertible polymersome by remarkably stable supramolecular assembly of naphthalene diimide (NDI) $\pi$-system. *Macromolecules 46*, 3939−3949.
(46) Shao, H., Nguyen, T., Romano, N. C., Modarelli, D. A., and Parquette, J. R. (2009) Self-assembly of 1-D n-type nanostructures based on naphthalene diimide-appended dipeptides. *J. Am. Chem. .Soc. 131*, 16374−16376.
(47) Shao, H., and Parquette, J. R. (2010) A $\pi$-conjugated hydrogel based on an fmoc-dipeptide naphthalene diimide semiconductor. *Chem. Commun. . 46*, 4285−4287.
(48) Das, A., and Ghosh, S. (2014) Supramolecular assemblies by charge-transfer interactions between donor and acceptor chromophores. *Angew. Chem., Int. Ed. 53*, 2038−2054.
(49) Vadehra, G. S., Wall, B. D., Diegelmann, S. R., and Tovar, J. D. (2010) On-resin dimerization incorporates a diverse array of $\pi$-conjugated functionality within aqueous self-assembling peptide backbones. *Chem. Commun. 46*, 3947−3949.
(50) Kar, H., Molla, M. R., and Ghosh, S. (2013) Two-component gelation and morphology-dependent conductivity of a naphthalene-diimide (NDI) $\pi$-system by orthogonal hydrogen bonding. *Chem. Commun. 49*, 4220−4222.
(51) Tovar, J. D. (2013) Supramolecular construction of optoelectronic biomaterials. *Acc. Chem. Res. 46*, 1527−1537.
(52) Ryan, D. M., and Nilsson, B. L. (2012) Self-assembled amino acids and dipeptides as noncovalent hydrogels for tissue engineering. *Polym. Chem. 3*, 18−33.
(53) Ma, M., Kuang, Y., Gao, Y., Zhang, Y., Gao, P., and Xu, B. (2010) Aromatic-aromatic interactions induce the self-assembly of pentapeptidic derivatives in water to form nanofibers and supramolecular hydrogels. *J. Am. Chem. Soc. 132*, 2719−2728.

(54) Gawronski, J., Brzostowska, M., Kacprzak, K., Kolbon, H., and Skowronek, P. (2000) Chirality of aromatic bis-imides from their circular dichroism spectra. *Chirality 12*, 263−268.
(55) Ruzza, P., Biondi, B., Marchiani, A., Antolini, N., and Calderan, A. (2010) Cell-penetrating peptides: a comparative study on lipid affinity and cargo delivery properties. *Pharmaceuticals 3*, 1045−1062.
(56) Uchida, K., Yamaguchi, S., Yamada, H., Akazawa, M., Katayama, T., Ishibashi, Y., and Miyasaka, H. (2009) Photoisomerization of an azobenzenegel by pulsed laser irradiation. *Chem. Commun.*, 4420−4422.
(57) Tang, C., Ulijn, R. V., and Saiani, A. (2011) Effect of glycine substitution on fmoc−diphenylalanine self-assembly and gelation properties. *Langmuir 27*, 14438−14449.
(58) Wang, X. Z., Li, X. Q., Shao, X. B., Zhao, X., Deng, P., Jiang, X. K., Li, Z. T., and Chen, Y. Q. (2003) Selective rearrangements of quadruply hydrogen-bonded dimer driven by donor−acceptor interaction. *Chem.—Eur. J. 9*, 2904−2913.